Effects of Contents of Multiwall Carbon Nanotubes in Polyaniline Films on Optical and Electrical Properties of Polyaniline

N. Bafandeh[1], M. M. Larijani[2**], A. Shafiekhani[3,4], M. R. Hantehzadeh[1], N. Sheikh[2]

[1]*Department of Physics, Science and Research Branch, Islamic Azad University, Tehran, Iran*
[2]*Nuclear Radiation Applications Research School, Nuclear Science and Technology Research Institute, Tehran, Iran*
[3]*Physics Department, Alzahra University, Tehran, Iran*
[4]*School of Physics, Institute for Research in Fundamental Sciences, Tehran, Iran*

(Received 30 June 2016)

We investigate the effects of different contents of multiwall carbon nanotubes (MWCNTs) on optical and electrical properties of polyaniline (PANI). The MWCNTs/PANI composites are deposited on glass substrates coated with indium tin oxide (ITO) by the spin-coating technique. The scanning electron microscopy shows that nanotubes are coated with the PANI layer and x-ray diffraction patterns show that all deposited composite films have an amorphous character. The analysis of a UV-vis spectrophotometer indicates the blue shift of the absorbance peak and a decrease in optical band gap value by the enhancement of the CNT content in the PANI matrix while the Urbach energy increases. The Raman spectrum shows the blue shift 1404→1417 cm^{-1} and photoluminescence spectra show an increase in the intensity of characteristic PANI peak at 436 nm with the increasing CNT content.

PACS: 78.20.−e, 82.35.Lr, 61.82.Pv, 64.70.pj DOI: 10.1088/0256-307X/33/11/117801

Polyaniline is one of the most attractive conductive polymers due to its high chemical, environmental and thermal stability up to 420℃, low cost, ease of synthesis, high electrical conductivity and simple doping/dedoping chemistry.[1−4] Recently, nanomaterials have been studied by many researchers due to their industrial applications.[5−8] On the other hand, carbon nanotubes (CNTs) have extraordinary electrical and mechanical properties due to their unique atomic structure. The large surface area provided by the hollow cores and outside walls of nanotubes makes them applicable as a gas sensor.[9] The formation of PANI/CNT composites can improve the electrical, optical and gas sensing properties of polyaniline. CNTs can increase the number of interacting sites for sensing different gases. The charge transfer between PANI and CNT can enhance their electronic interaction.[9] PANI/CNT composites have wide applications in fuel cells,[10,11] solar cells,[12] photovoltaic devices, sensors and biosensors,[13,14] thermoelectric devices,[15] functional membranes,[16] capacitors,[17] and artificial muscles.[18]

In this Letter, composites based on multiwall carbon nanotubes (MWCNTs) and doped PANI are prepared with the solution mixing method and spin coated on indium tin oxide (ITO) coated glass. We aim to study the effect of different CNT contents on PANI's optical, structural and morphological properties.

Aniline (99%), hydrochloric acid HCL (36%), 10-camphorsulfonic acid (CSA), ammonium peroxide sulfate (99%), chloroform (99.9%), ammonia solution (25%), multiwall carbon nanotubes (purity>95%, length∼30 μm and OD<8 nm) and ITO-coated glass (80 nm ITO on glass with 8 sheet resistivity) were used.

Synthesis of polyaniline was performed by chemical oxidative polymerization of 0.3 M aniline in 1 M HCl solution and dropwise addition of $(NH_3)_2S_2O_8$ in the same molar ratio to aniline for 2 h with stirring continuously at 0–5. The solution was refined and the product was washed with 1 M HCl and dried under vacuum for 24 h. The resulting product was emeraldine salt (ES) form of polyaniline. PANI HCl powder remained in 0.1 M ammonia solution and was stirred for 6 h at room temperature. The chemical sediment was refined and washed, respectively, then was dried in vacuum for 24 h to attain emeraldine base (EB) PANI.

PANI was mixed with acid sulfonic camphor (CSA) as a strong acid for protonation of EB PANI, while ES form is not directly soluble in any organic solvent.[19] The mixture was dissolved in 12 mL chloroform and stirred continuously by magnetic stirrer for 6–7 days. MWCNTs (1, 2, 4 wt%) were separately dispersed in 5 ml chloroform by ultrasonication for 2 h. This solution was dispersed in prepared doped PANI solution by using ultrasonication for 30 min. Pre-production solution was deposited on ITO-coated glass (1×1 cm^2) as a substrate by the spin coating technique at a speed of 2500 rpm. Before use, the substrate was ultrasonically cleaned in heated acetone and ethanol solutions. The spin coated film was dried at 60℃ in the vacuum for 1 h. The obtained composite thin films with 1, 2 and 4 wt% of MWCNTs were denoted as PC1, PC2 and PC3, respectively.

The UV-vis spectra were obtained by using a Varian Cary-500 spectrophotometer. Photoluminescence properties of the samples were studied by a Cary Eclipse spectrometer equipped with a xenon lamp at

**Corresponding author. Email: mmojtahedfr@yahoo.com
© 2016 Chinese Physical Society and IOP Publishing Ltd

room temperature. The morphology was characterized by scanning electron microscopy (SEM) (KYKY-EM3200). Raman spectra were recorded by using a Thermo Nicolet (960, USA). An atomic force microscope (AFM) was used to study the surface topography of the CNT/PANI composite films.

The typical SEM image of the PC2 sample containing 2 wt% MWCNTs in PANI is shown in Fig. 1. The MWCNTs are obviously seen in the SEM image as large bundles of tangled carbon nanotubes covered by polymer. A large number of porosity defects are present on the composite surface, which suggests its application as gas sensors based on porous semiconductors.

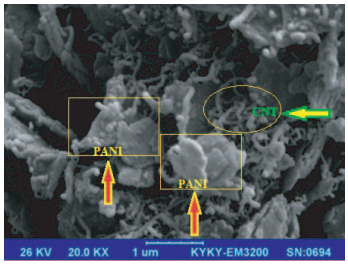

Fig. 1. Typical SEM image of PC2.

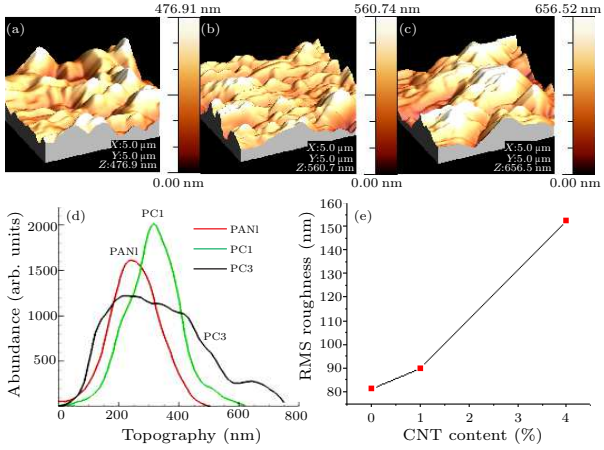

Fig. 2. AFM pictures of (a) PANI, (b) PC1, (C) PC3, (d) abundance of topography and (e) rms roughness of samples.

To investigate the surface topography, atomic force microscopy (AFM) studies have been carried out for PANI and MWCNT/PANI composite films. Figures 2(a)–2(c) show the three-dimensional AFM images of PANI, PC1 and PC3 films, respectively, for a surface of 5 μm × 5 μm. The abundance of topography for different samples is shown in Fig. 2(d). Distribution of particle sizes on the surface of PANI and PC1 films is presented by a perfect Gaussian line indicating nearly uniform surface topography. However, the particle size distribution in the PC4 film is not quite a perfect Gaussian line. Figure 2(e) shows the rms roughnesses of PANI, PC1 and PC3. An increase of surface roughness is observed by increasing the amount of CNTs in the composite film.

Figure 3 shows the XRD pattern of the PC3 sample (4 wt% of CNTs) on ITO-coated glass. The peaks at 2O–30, 35, 50 and 60 are related to the ITO film coated glass.[20] There is no clear peak corresponding to PANI and CNTs in XRD patterns. Similar results are observed for all the samples prepared in this investigation confirming the amorphous nature of the prepared composite.

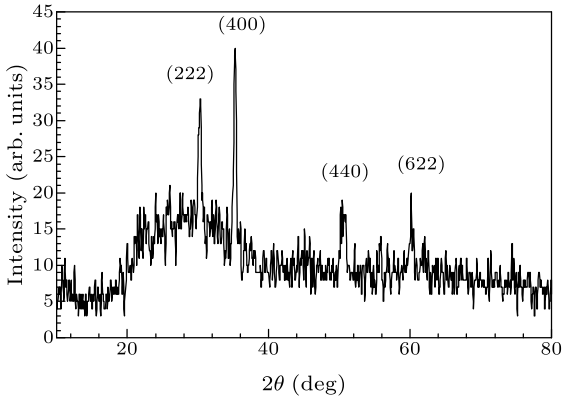

Fig. 3. XRD pattern of the PC3 film on the ITO-coated glass.

UV-vis absorption spectra of all the samples are shown in Fig. 4. The characteristic absorption peaks of PANI appear in 347, 404 and 731 nm, which are due to π–π^*, polaron–π^* and π–polaron transitions, respectively.[18,21]

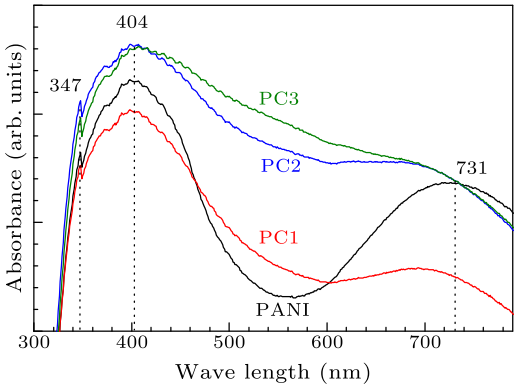

Fig. 4. UV-vis absorbance spectra of (a) PANI, (b) PC1, (c) PC2 and (d) PC3.

Figure 4 shows a blue shift from PANI to PCs at 731 nm. This shift could be due to redistribution of polaron density in the band gap of PANI due to the impact of CNTs[19] and also because of the increase of the interaction energy caused by interaction of polyaniline with MWCNTs.[22] Moreover, the increase of CNTs in PANI causes a continuous absorption of incident light from 404 to 731 nm, which means an increase of localized state density within the band gap.

Bandgaps of pure PANI and PCs are calculated by using the Tauc equation[19] given by

$$\alpha h\nu = A(h\nu - E_{\rm g})^n, \qquad (1)$$

where E_g, α, A and $h\nu$ are the bandgap energy, the absorption coefficient, the proportionality constant and the photon energy, respectively, and n is the index having the values of $\frac{1}{2}$, $\frac{3}{2}$, 2 and 3 depending on the mode of transition. Band gaps of PANI and PCs are shown in Fig. 5 considering a direct transition for $n = \frac{1}{2}$.

Figure 5 indicates a decrease in the band gap by increasing the CNT content in composites from 3.44 eV for PANI to 3.40, 3.37 and 3.29 eV for PC1, PC2 and PC3, respectively, which can be assigned to the interaction of MWCNTS with PANI,[22] which creates sub-band states in the PANI band gap accompanied by a narrowing of the band gap.[24]

In amorphous materials a dense localized state can exist between valence and conduction bands called the Urbach energy (or the Urbach tail) due to the structural disorder. The Urbach energy is related to the width of the tails of localized state and indicates the grade of disorder in the amorphous semiconductors.[25]

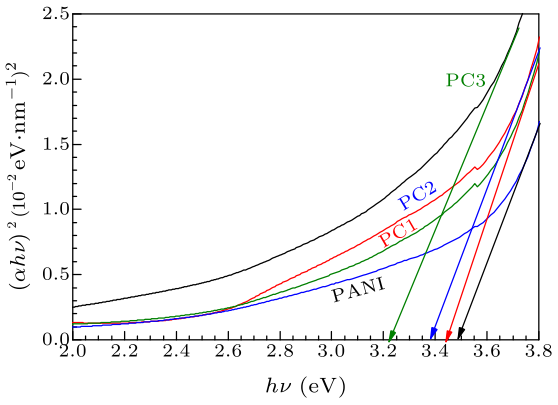

Fig. 5. Bandgap calculation of (a) PANI, (b)PC1, (c) PC2 and (d) PC3 films.

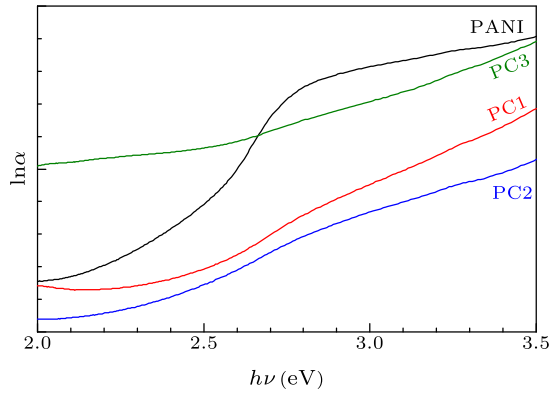

Fig. 6. The Urbach tail changes for (a) PANI and (b) PC1, (c) PC2 and (d) PC3.

At lower photon energy the Urbach rule is dominant on absorption as follows:

$$\alpha(h\nu) = \alpha_0 \exp(h\nu/E_u), \tag{2}$$

where α_0 and E_u are a constant and the Urbach energy, respectively. The inverse of the slope of $\ln\alpha$ as a function of $(h\nu)$ (as shown in Fig. 6) gives E_u. The calculated E_u are 0.8, 1.16, 1.5 and 2 eV for PANI, PC1, PC2 and PC3, respectively.

The obtained values of the Urbach energies and bandgap energies are compared as shown in Fig. 7, which indicates the antithetic behavior of these energies by increasing the CNT content. This figure shows that the Urbach energy increases with the CNTs, which results in the rise of localized state formation in PANI chain.[24]

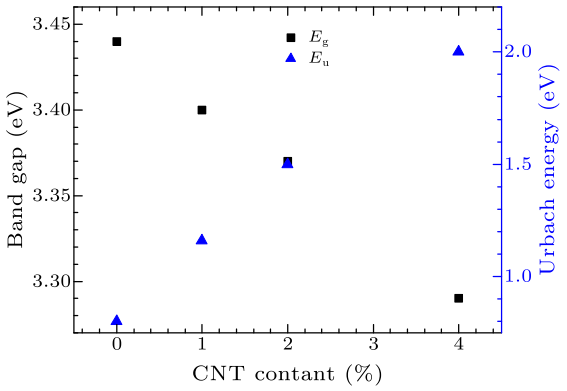

Fig. 7. Variation of the band gap energy (E_g and the Urbach energy (E_u) as a function of the CNT content.

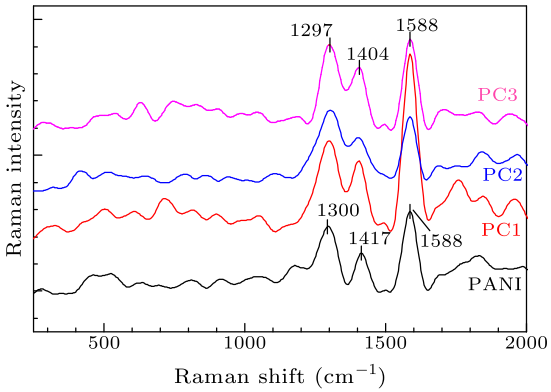

Fig. 8. Raman spectra of (a) PANI, (b) PC1, (c) PC2 and (d) PC3 samples.

Figure 8 shows the Raman spectra of PANI and PC composites. Characteristic Raman shifts of PANI are located at 1300, 1417 and 1588 cm^{-1}, which are assigned to C–N$^+$,[26] C–C stretching and C=C stretching vibration,[27] respectively. Figure 8 shows a 13 cm^{-1} blue shift of 1404→1417 cm^{-1} from PANI to PC3, which is due to π–π^* electron interaction between PANI and MWCNTS.[26] The intensity and width of Raman peak are also increased by increasing the CNT content.

PL spectroscopy of PANI and PC composites in the range of 400–500 cm^{-1} is depicted in Fig. 9. The excitation wavelength is taken as 350 nm for all the samples at room temperature, due to the benzenoid π–π^* transitionary.[28,29] As shown in Fig. 9, the emission peak is observed at 436 nm, which is assigned to the transition from the polaron band to the band

structure of PANI.[30] The intensity of the Pl spectrum is obviously increased by increasing the CNT content due to the higher extent of π-conjugation in nanocomposites.[22] The variation of PL peaks' area as a function of the CNT content in Fig. 10 clearly indicates that the increase in the CNT content leads to an increase in the PL peak area, which is correlated to the amount of density of trap states.[31]

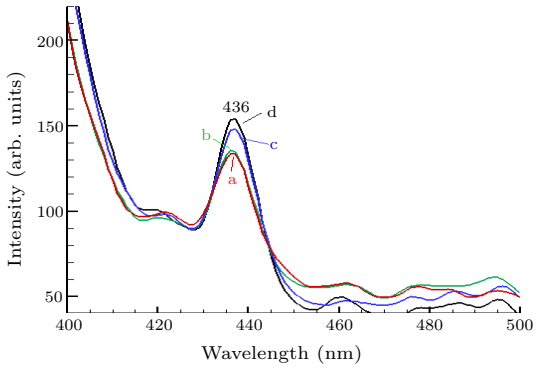

Fig. 9. Photoluminescence spectra of (a) PANI, (b) PC1, (c) PC2 and (d) PC3.

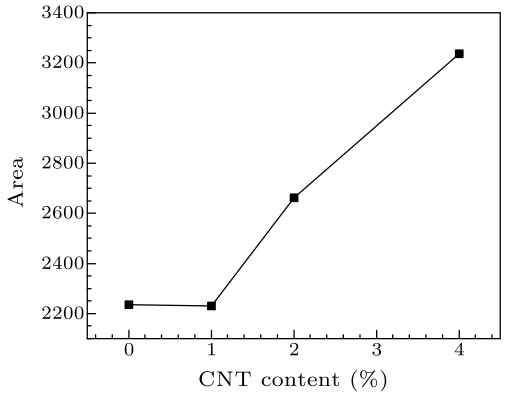

Fig. 10. Variation of PL peak area as a function of the CNT content.

In summary, effects of different CNT contents on optical, structural and morphological properties of CSA-doped PANI have been studied. The SEM image clearly indicates the presence of CNTs in the composite. The AFM results show that the increasing amount of CNT ends in the increase of the rms roughness. The UV-vis spectroscopy presents two absorbance peaks related to PANI in all the samples and the blue shifts appear in the composites due to the impact of added CNTs. The band gap value decreases and the Urbach energy increases with the increasing CNT content, which are assigned to the rise of localized states in PANI chains. The Raman spectroscopy shows the characteristic peaks of PANI for all the samples. The blue shift is depicted in the Raman spectrum, which is due to the π–π^* electron interaction between PANI and MWCNTs. The photoluminescence spectroscopy exhibits that the emission wavelengths of all the samples are centered at 436 nm, and the intensities of the emission peaks are increased with the rise of the CNT content due to the higher extent of conjugation in nanocomposites.

References

[1] Palaniappan S and John A 2008 *Prog. Polym. Sci.* **33** 732
[2] Zhang X, Ji L, Zhang S and Yang W 2007 *J. Power Sources* **173** 1017
[3] Kulkarni V G, Campbell L D and Mathew W R 1989 *Synth. Met.* **30** 321
[4] Heeger A J 2001 *Rev. Mod. Phys.* **73** 681
[5] Tălu Ş Solaymani S, Bramowicz M, Naseri N, Kulesza S and Ghaderi A 2016 *RSC Adv.* **6** 27228
[6] Stach S, Garczyk, Tălu Ş Solaymani S, Ghaderi A, Moradian R, Nezafat Negin B, Elahi S M and Gholamali H 2015 *J. Phys. Chem.* C **119** 17887
[7] Tăl Ş Bramowicz M, Kulesza S, Solaymani S, Shafikhani A, Ghaderi A and Ahmadirad M 2016 *J. Ind. Eng. Chem.* **35** 158
[8] Tălu Ş Bramowicz M, Kulesza S, Shafiekhani A, Ghaderi A, Mashayekhi F and Solaymani S 2015 *Ind. Eng. Chem. Res.* **54** 8212
[9] Srivastavaa S, Sharma S S, Kumar S, Agrawal Sh, Singh M and Vijay Y K 2009 *Int. J. Hydrogen Energy* **34** 8444
[10] Lin, Y, Cui, X, Yen, C H and Wai C M 2005 *Langmuir* **21** 11474
[11] Lee H, Rim H, Lee J Y, Lee J, Yoon J, Bae W and Yang S 2008 *J. Nanosci. Nanotechnol.* **8** 5464
[12] Ikeda N, Teshima K and Miyasaka T 2006 *Chem. Commun.* **16** 1733
[13] Singh R, Dhand C, Sumana G, Verma R, Sood S, Gupta R K and Malhotra B D 2010 *J. Mol. Recognit.* **23** 472
[14] Ben-Valid S, Dumortier H, Decossas M, Sfez R, Meneghetti M, Bianco A and Yitzchaik S 2010 *J. Mater. Chem.* **20** 2408
[15] Yao Q, Chen L D, Zhang W Q, Liufu S C and Chen X H 2010 *ACS Nano* **4** 2445
[16] Panhuis M I H, Doherty K J, Sainz R, Benito A M and Maser W K 2008 *J. Phys. Chem.* C **112** 1441
[17] Zhou Y, Qin Z Y, Li L, Zhang Y, Wei Y L, Wang L F and Zhu M F 2010 *Electrochim. Acta* **55** 3904
[18] Haspulat B, Gulce A and Gulce H 2013 *Hazardous Mater.* **260** 518
[19] Nasirian S and Milani M H 2014 *Int. J. Hydrogen Energy* **39** 630
[20] Choi D, Hong S and Son Y 2014 *Materials* **7** 7662
[21] Patil S L, Chougule M A, Pawar S G, Sen S and Patil V B 2012 *Soft Nanosci. Lett.* **2** 46
[22] Chakraborty G, Gupta K, Rana D and Meikap A K 2012 *Adv. Nat. Sci.: Nanosci. Nanotechnol.* **3** 035015
[23] Subramanian S and Padiyan D P 2008 *Mater. Chem. Phys.* **107** 392
[24] Choudhury B, Dey M and Choudhury A 2013 *Int. Nano Lett.* **3** 25
[25] Tauc J 1974 *Amorphous and Liquid Semiconductors* (London: Plenum Press)
[26] Yuan B, Yu L, Sheng L, An K and Zhao X 2012 *J. Phys.* D **45** 235108
[27] Zhang J, Liu C and Shi G 2005 *J. Appl. Polym. Sci.* **96** 732
[28] Urbach B, Korbakov N, Bar-David Y, Yitzchaik S and Sa'ar A 2007 *J. Phys. Chem.* C **111** 16586
[29] Babu V J, Vempati S and Ramakrishna S 2013 *Mater. Sci. Appl.* **4** 1
[30] Devi M R, Lawrence B, Prithivikumaran N and Jeyakumaran N 2014 *Chem. Tech. Res.* **13** 5400
[31] Gfroerer T H 2000 *Encyclopedia of Analytical Chemistry* (Chichester: John Wiley & Sons) p 9209